PERGAMON

International Journal of Heat and Mass Transfer 42 (1999) 455–465

International Journal of HEAT and MASS TRANSFER

A unified solution for heat conduction in thin films

Kathy J. Hays-Stang, A. Haji-Sheikh*

The University of Texas at Arlington, Department of Mechanical and Aerospace Engineering, Arlington, TX 76019-0023, U.S.A.

Received 4 September 1997; in final form 21 May 1998

Abstract

Mathematical formulations of heat conduction in thin films and subsequent analytical solutions are the subject of this paper. A generalized formulation of the energy equation that allows for local nonequilibrium conditions between the heat carriers is valid for a broad spectrum of materials from conductors to nonconductors. A unified solution is derived from the classical solution of the energy equation and it is cast as a modification of the Green's function solution for Fourier heat conduction. Numerical examples show the influence of periodic surface heat flux on phase angle and temperature, and the condition for lumped system approximation.

Nomenclature

C $C_e + C_l$ [J m^{-3} K^{-1}]
$\bar{C}$ C_e/C
C_e, C_l heat capacities [J m^{-3} K^{-1}]
G electron–phonon coupling
$\bar{G}$ GL^2/K
$G^M(\cdot)$ microscale Green's function
K thermal conductivity [W m^{-1} K^{-1}]
L film thickness [m]
m, n indices
q heat flux [W m^{-2}]
q_0 heat flux [W m^{-2}]
r position vector
S volumetric heat source [W m^{-3}]
S_n^* see equation (16c)
Sp speed number, $\sigma L/\alpha$
T temperature [K]
t time [s]
t_o period of oscillation [s]
t_p pulse period [s]
x coordinate [m].

Greek symbols

α thermal diffusivity [m^2 s^{-1}]
β_n parameter related to γ_n, equation (16a)
γ_n eigenvalue
λ_n parameter related to γ_n, equation (16b)
μ $(\tau_q + \tau_e)/\tau_t$
ν $2\pi \times$ frequency [rad s^{-1}]
ξ distance parameter, in equation (22)
σ thermal wave speed [m s^{-1}]
τ dummy variable and Green's function parameter
τ_e lag time, energy equation [s]
τ_F electron relaxation time [s]
τ_q lag time, heat flux [s]
τ_t lag time, temperature [s].

Subscripts

a, b, c conjugates of $G^M(\cdot)$
e electron
l lattice.

1. Introduction

Short-pulse energy deposition on thin films is used in micromachining, laser processing of diamond films, laser surface hardening, and other applications. Short-pulse lasers are also used in laboratories for evaluating the properties of thin films. Classical methods of predicting temperature lose validity for objects with length the order of a micron (or less) and for time the order of picoseconds (or less), when different models known as microscale heat transfer become necessary. For microscale heat transfer, the individual heat carriers, e.g., phonons, electrons, and photons, may dramatically affect the observed temperature behavior. In metals, both free electrons and phonons transfer heat energy while, in semiconductors,

* Corresponding author.

0017–9310/98 $19.00
PII: S0017–9310(98)00184–7

the phonons are the major heat carriers. The individual heat carriers travel an average distance, or mean free path, in a material before transmitting their energy to other heat carriers by collisions. The scattering of energy carriers by phonons, impurities, and various imperfections determines the state of energy transport [1].

There are different theories that predict the thermal behavior of thin metals and nonmetals. It is understood that electromagnetic radiation, ranging from ultraviolet to infrared, excites electrons in metals followed by electron–phonon interaction [2]. Photons excite electrons into higher energy levels. The excited electrons rapidly become thermalized producing a hot free electron gas. The electron gas diffuses through the metal lattice, generating phonons by colliding with the lattice (electron–phonon collisions); the mean collision time is small, of the order of 20 femtoseconds. The exchange of energy between electrons and phonons requires many collisions; therefore, the electron thermal relaxation time is in picoseconds. Qui and Tien [2, 3] used a two-step radiation-heating model to study absorption of photon energy by electrons and subsequent heating of the lattice through electron–phonon coupling.

The Boltzmann transport theorem is usually modified to obtain linear systems [3] to study various energy transport phenomena in microscale devices. The hyperbolic two-step radiation-heating model approximately describes the variation of temperature fields in thin metals due to electron gas flow and electron–lattice coupling. This model can be reduced to the parabolic two-step model.

The objective of this paper is to provide a complete solution of the microscale energy equation without limiting this solution to a specific material. This paper also includes a discussion of the derivation of the microscale energy equation without using quantum mechanics. This equation employs a lagging behavior similar to that reported in ref. [4] and agrees with the hyperbolic two-step model for metals [3]. It is remarkable that the exact solution of this equation can be constructed using the widely available Green's function solutions. The analysis leads to an interesting criterion that signifies the occurrence of a thermal wave. Two numerical examples are selected to validate the solution technique and to show the effect of various dimensionless variable groups on temperature for a range of sinusoidal heat input frequencies. A knowledge of the temperature response to a range of heat input frequencies is useful when studying the influence of a multifrequency energy source, e.g., a laser pulse, on temperature.

2. Analysis

The mathematical derivation of the energy equation presented is based on the hypothesis that energy input is absorbed by electrons and lattice in a substance. If a material has free electrons, the electrons can be considered separately and, at a given time, t, the electron gas temperature, $T_e(t)$, is different from the lattice temperature, $T_l(t)$; however, they are related [2, 3] by equation,

$$C_l \frac{\partial T_l(t)}{\partial t} = G[T_e(t) - T_l(t)] \tag{1}$$

that can be written as

$$T_e(t) = T_l(t) + \frac{C_l}{G}\frac{\partial T_l(t)}{\partial t}. \tag{2}$$

Equation (2) states that the temperatures of electron gas and lattice are related and this relation is described using the first two terms of the Taylor series.

2.1. Derivation of energy equation

Energy balance applied to an elemental volume at location $\mathbf{r}$ and at time t must include the contributions of the energy storage of the electron gas and the lattice, that is,

$$-\nabla\cdot\mathbf{q}(\mathbf{r},t) + S(\mathbf{r},t) = C_e\frac{\partial T_e(\mathbf{r},t)}{\partial t} + C_l\frac{\partial T_l(\mathbf{r},t)}{\partial t}. \tag{3a}$$

All subsequent formulations of the energy equation are based on equation (3a). Tzou [4] presented an equation similar to equation (3a) without including the electron energy storage. The parameters C_e and C_l are the volumetric heat capacities of electron gas and lattice, respectively. In the remaining steps of these derivations, the thermophysical properties are regarded as constant. Substitution of T_e from equation (2) into equation (3a) yields

$$\begin{aligned}-\nabla\cdot\mathbf{q}(\mathbf{r},t) + S(\mathbf{r},t) &= C\frac{\partial T_l(\mathbf{r},t)}{\partial t} + \frac{C_eC_l}{G}\frac{\partial^2 T_l(\mathbf{r},t)}{\partial t^2}\\ &= C\frac{\partial T_l}{\partial t} + C\tau_e\frac{\partial^2 T_l(\mathbf{r},t)}{\partial t^2}\end{aligned} \tag{3b}$$

where $C = C_e + C_l$ and $\tau_e = C_eC_l/GC$. The variable τ_e is the thermalization time in [3] and the lag time in [5].

Under the local equilibrium condition, the Fourier equation relates the heat flux, $\mathbf{q}$, to temperature according to equation,

$$\mathbf{q}(\mathbf{r},t) = -K\nabla T(\mathbf{r},t). \tag{4}$$

At time t, the system is not at the state of equilibrium. Before the onset of equilibrium, Tzou [4] used a dual lag time concept and rewrote equation (4) as

$$\mathbf{q}(\mathbf{r},t+\tau_q) = -K\nabla T_l(\mathbf{r},t+\tau_t) \tag{5}$$

where τ_t and τ_q are two independent lag times in equation (5). Expanding equation (5) in the Taylor series and retaining the first two terms of the series yields [4],

$$\mathbf{q}(\mathbf{r},t) + \tau_q\frac{\partial\mathbf{q}(\mathbf{r},t)}{\partial t} = -K\nabla T_l(\mathbf{r},t) - K\tau_t\frac{\partial}{\partial t}\nabla T_l(\mathbf{r},t) \tag{6a}$$

Alternatively, combining the microscopic heat flux equation [3], developed for metals, with equation (2), leads to the following relation,

$$\mathbf{q}(\mathbf{r},t)+\tau_F\frac{\partial\mathbf{q}(\mathbf{r},t)}{\partial t} = -K\nabla T_e(\mathbf{r},t)$$

$$= -K\nabla T_l(\mathbf{r},t)-K\frac{C_l}{G}\frac{\partial}{\partial t}\nabla T_l(\mathbf{r},t). \quad (6b)$$

Equation (6a) reduces to equation (6b) if $\tau_q=\tau_F$ and $\tau_t=C_l/G$.

Next, the focus is on the derivation of the energy equation. In subsequent formulations, T stands for T_l. Differentiating equation (3b) with respect to t and allowing the operator $(\nabla\cdot)$ to differentiate equation (6a) results in the following set of equations.

$$-\frac{\partial[\nabla\cdot\mathbf{q}(\mathbf{r},t)]}{\partial t}+\frac{\partial S(\mathbf{r},t)}{\partial t}=C\frac{\partial^2T(\mathbf{r},t)}{\partial t^2}+C\tau_e\frac{\partial^3T(\mathbf{r},t)}{\partial t^3} \quad (7)$$

$$\nabla\cdot\mathbf{q}(\mathbf{r},t)+\tau_q\nabla\cdot\left[\frac{\partial\mathbf{q}(\mathbf{r},t)}{\partial t}\right] = -\nabla\cdot[K\nabla T(\mathbf{r},t)]-\tau_t\nabla\cdot\left[\frac{\partial}{\partial t}K\nabla T(\mathbf{r},t)\right]. \quad (8)$$

By changing the order of differentiation, one can equate the terms

$$\frac{\partial[\nabla\cdot\mathbf{q}(\mathbf{r},t)]}{\partial t}=\nabla\cdot\left[\frac{\partial\mathbf{q}(\mathbf{r},t)}{\partial t}\right]$$

in equations (7) and (8) and after substituting for $\nabla\cdot\mathbf{q}(\mathbf{r},t)$ from equation (3b), the result is,

$$\nabla\cdot[K\nabla T(\mathbf{r},t)]+\tau_t\frac{\partial\{\nabla\cdot[K\nabla T(\mathbf{r},t)]\}}{\partial t} +\left[S(\mathbf{r},t)+\tau_q\frac{\partial S(\mathbf{r},t)}{\partial t}\right] = C\frac{\partial T(\mathbf{r},t)}{\partial t}+C(\tau_e+\tau_q)\frac{\partial^2T((\mathbf{r},t)}{\partial t^2} +C\tau_e\tau_q\frac{\partial^3T(\mathbf{r},t)}{\partial t^3}. \quad (9)$$

The formulations leading to equation (9) are based on physical reasoning and mathematical deductions. Qui and Tien [3], using quantum mechanics, developed a hyperbolic two-step model for metals that can also produce equation (9). A comparison with the derivations in [3] shows that parameter τ_q, for metals, is the same as τ_F, known as the electron relaxation time at the Fermi surface. To estimate parameters $\tau_t=C_l/G$, $\tau_e=C_eC_l/CG$, and τ_q, the typical values of C_e, C_l, G, and τ_F for selected metals are presented in Table 1. Based on data in Table 1, the parameters τ_t, τ_e, τ_q are quite small.

Below it is shown that the third partial derivative of temperature with respect to time in equation (9) is negligibly small when multiplied by τ_e and τ_q. The right-hand-side of equation (9) can be written as

$$C\frac{\partial T(\mathbf{r},t)}{\partial t}+C(\tau_e+\tau_q)\frac{\partial^2T(\mathbf{r},t)}{\partial t^2} +C\tau_e\tau_q\frac{\partial^3T(\mathbf{r},t)}{\partial t^3}=C\frac{\partial}{\partial t}\left[T(\mathbf{r},t)+(\tau_e+\tau_q)\frac{\partial T(\mathbf{r},t)}{\partial t} +\tau_e\tau_q\frac{\partial^2T(\mathbf{r},t)}{\partial t^2}\right]. \quad (10)$$

Now, the term in square brackets is compared with the Taylor series expansion $T[t+(\tau_e+\tau_q)]$,

$$T[t+(\tau_e+\tau_q)\cong T(\mathbf{r},t),t) +(\tau_e+\tau_q)\frac{\partial T(\mathbf{r},t)}{\partial t}+\frac{(\tau_e+\tau_q)^2}{2}\frac{\partial^2T(\mathbf{r},t)}{\partial t^2}.$$

This suggests, when $(\tau_e+\tau_q)$ is small, the following inequality holds,

$$\frac{(\tau_e+\tau_q)^2}{2}\frac{\partial^2T(\mathbf{r},t)}{\partial t^2}\ll(\tau_e+\tau_q)\frac{\partial T(\mathbf{r},t)}{\partial t}$$

indicating that the higher order term is negligible. Since τ_t and τ_e are real, then $\tau_t\tau_e<(\tau_e+\tau_q)^2/2$, and the term containing $\partial^3T/\partial t^3$, equation (9), should be discarded. The final form of the microscale thermal conduction equation is

$$\nabla\cdot[K\nabla T(\mathbf{r},t)]+\tau_t\frac{\partial\{\nabla\cdot[K\nabla T(\mathbf{r},t)]\}}{\partial t} +\left[S(\mathbf{r},t)+\tau_q\frac{\partial S(\mathbf{r},t)}{\partial t}\right] = C\frac{\partial T(\mathbf{r},t)}{\partial t}+C(\tau_e+\tau_q)\frac{\partial^2T(\mathbf{r},t)}{\partial t^2}. \quad (11)$$

Equation (11) is a more tractable version of equation (9) with no loss of generality; no reference is made to the number of spatial dimensions or to the type of materials studied. Using appropriate values of 'lag' times, τ_t, τ_e, τ_q, and other thermophysical properties, equation (11) holds for dielectric materials, conductors, or semiconductors. The analytical solution of this equation is new and it is useful for finding the temperature field for a broad range of microscale applications.

2.2. Solution

The analytical solution of this equation is an essential part of this presentation. The derivation begins by proposing a series solution for finite bodies of the form

$$T(\mathbf{r},t)=\sum_{n=1}^{\infty}\psi_n(t)F_n(\mathbf{r})\,e^{-\gamma_nt} \quad (12)$$

where $F_n(\mathbf{r})$ satisfies equation

$$\nabla\cdot[K\nabla F_n(\mathbf{r})]=-\gamma_nCF_n(\mathbf{r}) \quad (13)$$

Table 1
The electron–phonon coupling factors [2] heat capacity [6] and thermal conductivity [7]

Metal	G [TW m^{-3} K^{-1}]	C_e [MJ m^{-3} K^{-1}]	C_l [MJ m^{-3} K^{-1}]	K [W m^{-1} K^{-1}]	τ_F [ps]
Au	28 000	0.021	2.5	317	0.04
Ag	28 000	0.019	2.5	429	0.04
Cu	48 000	0.029	3.4	401	0.03
Cr	420 000	0.058	3.2	93.7	0.003
W	260 000	0.041	2.5	174	0.01
Pb	120 000	0.049	1.5	35.3	0.005

and homogeneous boundary conditions. Substitution of T from equation (12) in equation (11), multiplying both sides of the resulting equation by $F_m(\mathbf{r})$, and using the orthogonality condition,

$$\int_V F_n(\mathbf{r})F_m(\mathbf{r})\,\mathrm{d}V = \begin{cases} 0 & \text{when } n \neq m \\ N_n & \text{when } n = m \end{cases} \tag{14}$$

yields, in an ordinary differential equation, the relation

$$\frac{\mathrm{d}^2\psi_n(t)}{\mathrm{d}t^2} - 2\beta_n\frac{\mathrm{d}\psi_n(t)}{\mathrm{d}t} + \lambda_n^2\psi_n(t) = S_n^*(t). \tag{15}$$

The symbols β_n, λ_n, and $S_n^*(t)$ are short-hand notations defined by the relations,

$$\beta_n = \gamma_n\left[1 - \frac{1}{2}\frac{\tau_t}{\tau_q+\tau_e} - \frac{1}{2\gamma_n(\tau_q+\tau_e)}\right] \tag{16a}$$

$$\lambda_n = \gamma_n\left[1 - \frac{\tau_t}{\tau_q+\tau_e}\right]^{1/2} \tag{16b}$$

$$S_n^*(t) = \frac{\mathrm{e}^{\gamma_n t}}{N_n C(\tau_q+\tau_e)}\int_V F_n(\mathbf{r})\left(S(r,t) + \tau_q\frac{\partial S(\mathbf{r},t)}{\partial t}\right)\mathrm{d}V. \tag{16c}$$

It is remarkable that, except for coefficients β_n and λ_n, this solution of equation (15) is identical to that presented by Haji-Sheikh and Beck [8] for the thermal wave equation. Modifications are needed to account for the contribution of the terms in square brackets, equation (16a), and for the term $\tau_t/(\tau_q+\tau_e)$ in equation (16b). The solution [8] of equation (15) leads to the value of the function ψ as

$$\psi_n(t) = \mathrm{e}^{\beta_n t}\{D_{1n}\sinh[\sqrt{(\beta_n^2-\lambda_n^2)}t] + D_{2n}\cosh[\sqrt{(\beta_n^2-\lambda_n^2)}t]\} + \int_{\tau=0}^{t}\frac{\mathrm{e}^{\beta_n(t-\tau)}\sinh[\sqrt{(\beta_n^2-\lambda_n^2)}(t-\tau)]}{\sqrt{(\beta_n^2-\lambda_n^2)}}S_n^*(\tau)\,\mathrm{d}\tau. \tag{17}$$

The arguments of hyperbolic sine and cosines are real if $\beta_n^2-\lambda_n^2 > 0$; otherwise, they are imaginary; however, the quantity $\psi_n(t)$ is always real. The constants of integration are D_{1n} and D_{2n} that must be determined using the initial temperature $T_i(\mathbf{r}) = T(\mathbf{r},0)$ and $T_{ii}(\mathbf{r}) = \partial T(\mathbf{r},t)/\partial t$ as $t \to 0$. The substitution of $\psi_n(t)$ from equation (17) in equation (12) provides the complete solution for the homogeneous boundary conditions. The contribution of the initial condition is

$$T_I(\mathbf{r},t) = \sum_{n=1}^{\infty}\frac{F_n(\mathbf{r})}{N_n}\mathrm{e}^{-(\gamma_n-\beta_n)t}\left\{\frac{\sinh[\sqrt{(\beta_n^2-\lambda_n^2)}t]}{\sqrt{(\beta_n^2-\lambda_n^2)}}\times\left[(\gamma_n-\beta_n)\int_V F_n(\mathbf{r})T_i(\mathbf{r})\,\mathrm{d}V' + \int_V F_n(\mathbf{r})T_{ii}(\mathbf{r})\,\mathrm{d}V'\right] + \cosh[\sqrt{(\beta_n^2-\lambda_n^2)}t]\int_V F_n(\mathbf{r})T_i(\mathbf{r})\,\mathrm{d}V'\right\} \tag{18a}$$

and the contribution of the volumetric heat source is

$$T_S(\mathbf{r},t) = \sum_{n=1}^{\infty}\int_{\tau=0}^{t}\int_V\left(\frac{F_n(\mathbf{r})F_n(\mathbf{r}')}{CN_n}\right)\mathrm{e}^{-\gamma_n(t-\tau)}\times\left\{\frac{\mathrm{e}^{\beta_n(t-\tau)}\sinh[\sqrt{(\beta_n^2-\lambda_n^2)}(t-\tau)]}{(\tau_q+\tau_e)\sqrt{(\beta_n^2-\lambda_n^2)}}\right\}\times\left(S(\mathbf{r}',\tau)+\tau_q\frac{\partial S(\mathbf{r}',\tau)}{\partial\tau}\right)\mathrm{d}V'\,\mathrm{d}\tau. \tag{18b}$$

Then, the general solution for homogeneous boundary conditions is

$$T(\mathbf{r},t) = T_I(\mathbf{r},t) + T_S(\mathbf{r},t). \tag{18c}$$

The detailed procedure that includes the contribution of nonhomogeneous boundary conditions is in [8]. Also, this reference contains a method of calculating the Green's function from equation (18b) that is employed in the subsequent analysis.

If $S(\mathbf{r}',\tau)$ in equation (18b) is replaced by $C\delta(\tau-\tau^*)\delta(\mathbf{r}'-\mathbf{r}^*)$ and after some algebraic steps described in [8], the result is the Green's function

$$G^{\mathrm{M}}(\mathbf{r},t\,|\,\mathbf{r}',\tau) = G_a^{\mathrm{M}}(\mathbf{r},t\,|\,\mathbf{r}',\tau)$$

$$+\frac{\tau_q}{\tau_e+\tau_q}[G_b^{\mathrm{M}}(\mathbf{r},t\,|\,\mathbf{r}',\tau)-G_c^{\mathrm{M}}(\mathbf{r},t\,|\,\mathbf{r}',\tau)] \quad (19a)$$

where

$$G_a^{\mathrm{M}}(\mathbf{r},t\,|\,\mathbf{r}',\tau)=\sum_{n=1}^{\infty}\left(\frac{F_n(\mathbf{r})F_n(\mathbf{r}')}{N_n}\right)e^{-\gamma_n(t-\tau)} \times\left\{\frac{e^{\beta_n(t-\tau)}\sinh[\sqrt{(\beta_n^2-\lambda_n^2)}(t-\tau)]}{(\tau_q+\tau_e)\sqrt{(\beta_n^2-\lambda_n^2)}}\right\} \quad (19b)$$

and

$$G_b^{\mathrm{M}}(\mathbf{r},t\,|\,\mathbf{r}',\tau)=\sum_{n=1}^{\infty}\left(\frac{F_n(\mathbf{r})F_n(\mathbf{r}')}{N_n}\right)e^{-\gamma_n(t-\tau)} \times\{e^{\beta_n(t-\tau)}\cosh[\sqrt{(\beta_n^2-\lambda_n^2)}(t-\tau)]\} \quad (19c)$$

$$G_c^{\mathrm{M}}(\mathbf{r},t\,|\,\mathbf{r}',\tau)=\sum_{n=1}^{\infty}\left(\frac{F_n(\mathbf{r})F_n(\mathbf{r}')}{N_n}\right)e^{-\gamma_n(t-\tau)} \times\left\{(\gamma_n-\beta_n)\frac{e^{\beta_n(t-\tau)}\sinh[\sqrt{(\beta_n^2-\lambda_n^2)}(t-\tau)]}{\sqrt{(\beta_n^2-\lambda_n^2)}}\right\}. \quad (19d)$$

For dielectric materials, $G\to\infty$ then $\tau_e=0$ and $\tau_q(\gamma_n-\beta_n)=1/2$ and equation (19a) reduces to

$$G^{\mathrm{M}}(\mathbf{r},t\,|\,\mathbf{r}',\tau)=(1/2)G_a^{\mathrm{M}}(\mathbf{r},t\,|\,\mathbf{r}',\tau)+G_b^{\mathrm{M}}(\mathbf{r},t\,|\,\mathbf{r}',\tau)$$

wherein $G^{\mathrm{M}}(\cdot)$, $(1/2)G_a^{\mathrm{M}}(\cdot)$, and $G_b^{\mathrm{M}}(\cdot)$ correspond to $G_w(\cdot)$, $G_{wa}(\cdot)$ and $G_{wb}(\cdot)$ defined in ref. [8]. The complete Green's function solution form of equation (18a), describing the effects of initial conditions, is

$$T_{\mathrm{I}}(\mathbf{r},t)=\int_V G_c^{\mathrm{M}}(\mathbf{r},t\,|\,\mathbf{r}',\tau)T_i(\mathbf{r}')\,\mathrm{d}V' +(\tau_q+\tau_e)\int_V G_a^{\mathrm{M}}(\mathbf{r},t\,|\,\mathbf{r}',\tau)T_{ii}(\mathbf{r}')\,\mathrm{d}V' +\int_V G_b^{\mathrm{M}}(\mathbf{r},t\,|\,\mathbf{r}',\tau)T_i(\mathbf{r}')\,\mathrm{d}V' \quad (20a)$$

and equation (18b) for the volumetric heat source effect is

$$T_{\mathrm{S}}(\mathbf{r},t)=\frac{1}{C}\int_{\tau=0}^{t}\mathrm{d}\tau\int_V G_a^{\mathrm{M}}(\mathbf{r},t\,|\,\mathbf{r}',\tau) \times\left(S(\mathbf{r}',\tau)+\tau_q\frac{\partial S(\mathbf{r}',\tau)}{\partial\tau}\right)\mathrm{d}V'. \quad (20b)$$

Equation (20b) is the basic solution for most laser heating problems in microscale applications. Accordingly, the temperature solutions for many microscale systems are readily available by minor modification of the Green's functions and Green's function solutions for Fourier heat conduction. In the following numerical examples, this solution method is tested through computation of the temperature response due to a sinusoidal heat input. This type of response is of interest in signal processing. The contribution of the nonhomogeneous boundary conditions can be included using a linear transformation of temperature as described in [8].

3. Numerical examples

3.1. Example 1. Thermal wave model

The following analysis applies to a thin film of a dielectric material modeled as a plate, Fig. 1, whose surfaces at $x=0$ and $x=L$ are insulated, and the material domain is initially at zero temperature. For dielectric materials, $\tau_t=0$, subsequently $\tau_e=0$, and $\tau_q=\alpha/\sigma^2$ where α is thermal diffusivity and σ is the speed of the thermal wave [9, 10].

3.2. Solution

A solution for a similar problem with a narrower range of frequency parameters is in [11]. For homogeneous boundary conditions and zero initial condition, equation (18b) reduces to the temperature solution,

$$T(x,t)=\frac{\alpha}{K}\int_{\tau=0}^{t}\mathrm{d}\tau\int_0^L G_a^{\mathrm{M}}(x,t\,|\,x',\tau) \times\left[S(x',\tau)+\frac{\alpha}{\sigma^2}\frac{\partial S(x',\tau)}{\partial\tau}\right]\mathrm{d}x' \quad (21a)$$

The Green's function for this example is

$$G_a^{\mathrm{M}}(x,t\,|\,x',\tau)=2\sum_{m=0}^{\infty}\frac{2-\delta_{0m}}{L}\cos\left(\frac{m\pi x}{L}\right) \times\cos\left(\frac{m\pi x'}{L}\right)e^{-\sigma^2(t-\tau)/2\alpha}\,\frac{\sin[\sigma^2\bar{\lambda}_m(t-\tau)/2\alpha]}{\bar{\lambda}_m} \quad (21b)$$

where $\bar{\lambda}_m=\sqrt{4m^2\pi^2/Sp^2-1}$ and $Sp=\sigma L/\alpha$ is the dimensionless speed number. For this specific example, it is assumed the heat source is at $x=0$ and it is described by the relation $S(x,t)=\delta(x-0)q(t)$ wherein the Dirac Delta function, $\delta(x-0)=0$ when $x\neq 0$. After substituting for $S(x',\tau)$ and $G_a^{\mathrm{M}}(x,t\,|\,x',\tau)$ in equation (21b) and following integration of the term containing

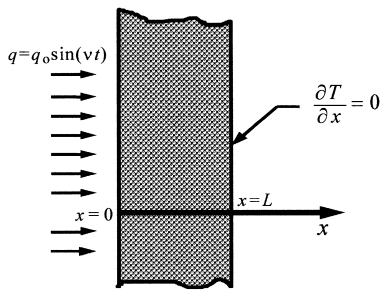

Fig. 1. Schematic of a thin plate and boundary conditions.

$\partial S(x',\tau)/\partial\tau$ by parts while assuming $q(0)=0$, equation (21a) reduces to

$$T=\frac{\alpha}{K\sigma}e^{-\sigma\xi/2\alpha}q(t-\xi/\sigma)+\frac{\alpha}{K}\sum_{m=0}^{\infty}\frac{2-\delta_{0m}}{L}\cos\left(\frac{m\pi x}{L}\right)\times\int_{\tau=0}^{t}e^{-\sigma^2(t-\tau)/2\alpha}\frac{\sin[\sigma^2\bar{\lambda}_m(t-\tau)/2\alpha]}{\bar{\lambda}_m}q(\tau)\,d\tau+\frac{\alpha}{K}\sum_{m=0}^{\infty}\frac{2-\delta_{0m}}{L}\cos\left(\frac{m\pi x}{L}\right)\int_{\tau=0}^{t}e^{-\sigma^2(t-\tau)/2\alpha}\times\{\cos[\sigma^2\bar{\lambda}_m(t-\tau)/2\alpha]-\cos[m\pi\sigma(t-\tau)/L]\}q(\tau)\,d\tau \quad (22)$$

where δ_{0m} is the Kronecker delta, $\delta_{0m}=1$ if $m=0$, otherwise $\delta_{0m}=0$. The first term on the right side of equation (22) describes the propagating thermal wave and contains a parameter, ξ, the distance that the wave travels, including boundary reflections. For thermal waves, reflections must be considered although the wave attenuates very quickly. The term containing ξ is obtained by integrating over the term with $\partial S(x',\tau)/\partial\tau$ in equation (20b). The unique feature of this solution is that the convergence of the last term in equation (22) is greatly enhanced because the term in square brackets goes to zero as $m\to\infty$.

The following parametric studies show the influence of a periodic surface heat flux on the amplitude and phase delay of the resulting temperature variation. For this initial parametric study, assume the surface heat flux is given as

$$q(\tau)=q_0\sin(vt) \quad (23)$$

where v is the angular frequency equal to $2\pi\times$ frequency and q is the heat flux with q_0 its amplitude. The dimensionless temperatures on both surfaces of the thin film are computed using equation (22). For comparison, the temperature is also calculated using the solution of the microscale conduction equation, e.g., equation (20b), see equation (A1) in appendix. An examination of the numerical results obtained from equation (22) and verified using equation (A1) shows that the former provides a better insight into the wave phenomena and has superior convergence characteristics. Figures 2–5 show the computed phase angle and dimensionless frequency using equation (22).

3.3. Results

To elucidate this presentation, an abstract thin film is chosen so that the value of the speed number, $Sp=\sigma L/\alpha$, is equal to five. Figure 2 is plotted for a dimensionless vL^2/α equal to 10. The temperature amplitude at $x=L$, for the thermal wave, equation (22), is the solid line in Fig. 2(b). It is slightly higher than the amplitude of

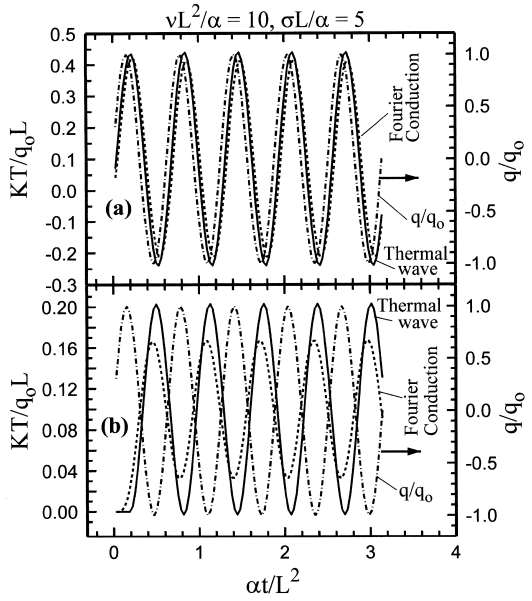

Fig. 2. Heat flux input at $x=0$ and temperature for thermal wave and Fourier conduction models when $vL^2/\alpha=10$ and $\sigma L/\alpha=5$; (a) at $x=0$ and (b) at $x=L$.

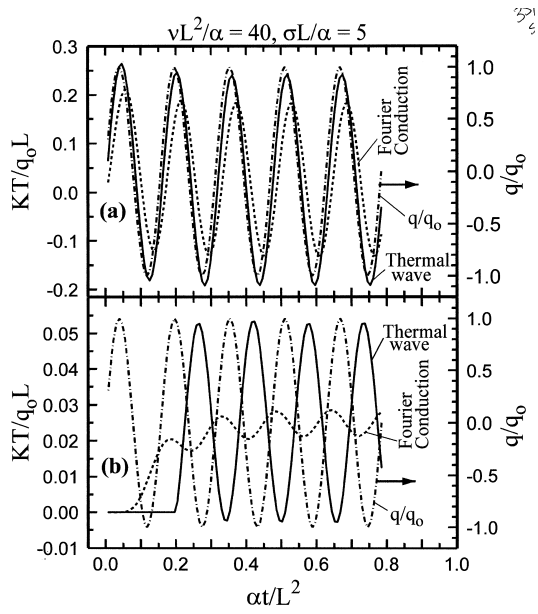

Fig. 3. Heat flux input at $x=0$ and temperature for thermal wave and Fourier conduction models when $vL^2/\alpha=40$ and $\sigma L/\alpha=5$; (a) = 0 and (b) at $x=L$.

temperature values, dash line, for the Fourier conduction and there is only a moderate change in the phase shift. In Fig. 2(a), at $x=0$, the graph shows that there is very

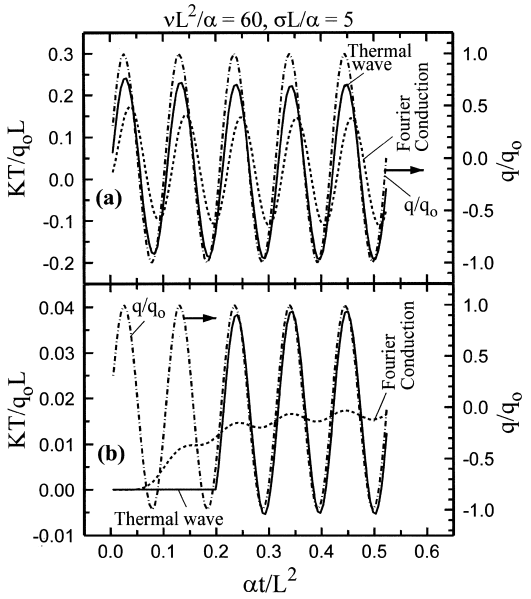

Fig. 4. Heat flux input at $x = 0$ and temperature for thermal wave and Fourier conduction models when $vL^2/\alpha = 60$ and $\sigma L/\alpha = 5$; (a) at $x = 0$ and (b) at $x = L$.

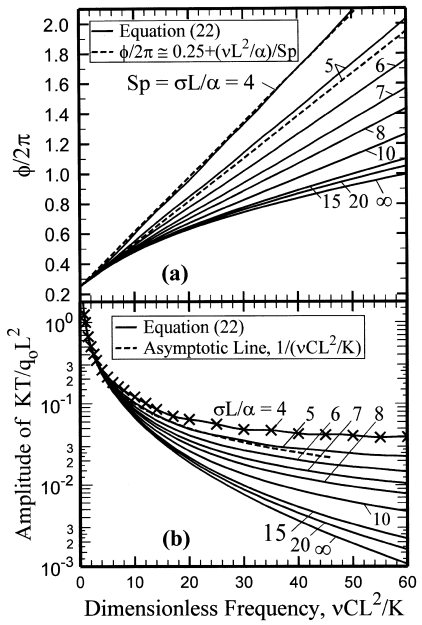

Fig. 5. Summary of (a) phase angle, (b) amplitude at $x = L$ different values of the $Sp = \sigma L/\alpha$.

little difference in the surface temperature using these two models.

Equation (22) shows that an increase in the frequency reduces the temperature amplitude at $x = L$; however, it will approach an asymptotic value. In contrast, in the Fourier conduction solution, the amplitude continuously reduces. These observations are graphically demonstrated, for $vL^2/\alpha = 40$ and 60, in Figs 3 and 4, respectively. As vL^2/α increases from 10 to 40, Fig. 3(b), the amplitude of temperature at $x = L$, for the thermal wave model, is reduced by a factor of ~ 4 and for the Fourier conduction model is reduced by a factor of nearly 13. Also, there is a significant increase in the phase shift for the thermal wave model at $x = L$. Figure 3(a) shows the temperature data at the $x = 0$ surface. As vL^2/α further increases, Fig. 4(b), clearly shows the effect of the thermal wave. There is only a moderate reduction of the temperature amplitude at $x = L$ for the thermal wave model while the phase delay spans over two periods. The data in Figs 3(b) and 4(b) show that there is an offset in the value of the mean temperature. For example, for the Fourier conduction and as $t \to \infty$, the value of this offset for dimensionless temperature, KT/q_0L, is equal to $1/(vL^2/\alpha)$.

To summarize the data, the value of the phase angle is plotted in Fig. 5(a) as a function of vL^2/α for different values of the speed number, $Sp = \sigma L/\alpha$. The ordinate in Fig. 5(a) is $\phi/2\pi$ where ϕ is the phase angle. The ordinate is also equal to the ratio of the time delay of the signal to the period of the signal, $\Delta t/t_o = \phi/2\pi$. In this figure, the $\sigma L/\alpha = \infty$ line represents the phase angle for the Fourier conduction model. The phase angle, ϕ, at the $x = L$ surface, for the thermal wave model is significantly larger than that for the Fourier heat conduction when $Sp = 5$, Fig. 5(a). This difference gradually diminishes as Sp increases to above 10. For Sp of below five, the thermal wave dominates and the first term on the right-hand-side of equation (22) plus an offset of ~ 0.25 adequately predicts the phase angle, $\phi \approx 0.25 + vx/\sigma$, see the dash lines in Fig. 5(a). The line for $Sp = 4$ shows a wavy behavior. This is unrelated to the series convergence since the '$\times$' symbols are computed symbolically using 100 terms and the solid lines are generated by Fortran using equation (22) and retaining as many as 40 000 terms. With no significant observed difference in the two calculated values, the wavy behavior is not due to numerical error. The corresponding amplitudes at the $x = L$ surface are plotted in Fig. 5(b). All amplitudes in Fig. 5(b) asymptotically approach $1/(vL^2/\alpha)$ when vL^2/α is less than one, see the dash line in Fig. 5(b). However, at large values of vL^2/α (not shown in the figure), the amplitude is higher for small Sp values and approaches the asymptotic value of $\exp(-Sp/2)/Sp$.

3.4. Example 2. Parametric studies of parabolic two-step model

The response of a thin metallic film to a periodic surface heat flux is considered. The computation of ampli-

tude and phase angle of a periodic surface heat flux is the subject of this example.

3.5. Solution

The response of a thin gold film to irradiation by a Gaussian-shaped light pulse has been examined analytically in [12] for the parabolic two-step model. The parabolic two-step model follows from the more general hyperbolic two-step equation by the elimination of $\tau_q = \tau_F$, assuming that it is small and it can be neglected. In the presence of a heat source, the generalized formulation for homogeneous boundary conditions and zero initial conditions, equation (18b), leads to a temperature solution for the parabolic two-step radiation heating model

$$T_1 = \frac{G}{C_e C_1} \sum_{m=0}^{\infty} \frac{2-\delta_{0m}}{L} \times \cos\left(\frac{m\pi x}{L}\right) \int_{\tau=0}^{t} e^{-(\gamma_m-\beta_m)(t-\tau)} \times \frac{\sinh[\sqrt{\beta_m^2-\gamma_m^2(1-C_1/C_e)}(t-\tau)]}{\sqrt{\beta_m^2-\gamma_m^2(1-C_1/C_e)}} d\tau \times \int_0^L \cos\left(\frac{m\pi x}{L}\right) S(x,\tau)\, dx \quad (24)$$

where $\gamma_m = (m\pi/L)^2 K/C$ and $\beta_m = \gamma_m[1-C/(2C_e)] - GC/(2C_eC_1)$. Recall that the electrons initially absorb the energy, move through the lattice and transfer their energy to the lattice. Furthermore, equation (A1) in the appendix yields the integrated form of equation (24) after appropriate substitutions for τ_e, τ_t, and letting $\tau_q \to 0$.

3.6. Results

Calculations of the phase angle presented here are for a typical range of significant parameter values. Of the significant parameters, only the ratio of electron and total heat capacities is solely determined by the material under consideration. The total heat capacity and the electron heat capacities are calculated by the method described in [6]. Care is taken that the $\bar{C} = C_e/C$ values in the calculations are typical for most metals. The values of $\bar{C}$, for data in Table 1, vary from 0.0075 for silver to 0.032 for lead. When necessary, the infinite series, in equation (24) is truncated at $M = 5000$, where M is the number of terms in the series. Generally, $M = 500$ terms resulted in four accurate significant figures.

The significant parameters that determine the phase response of the film to sinusoidal heat input are the dimensionless electron-phonon coupling factor, $\bar{G} = GL^2/K$, the ratio of electron to total heat capacities, $\bar{C} = C_e/C$, and the Fourier dimensionless frequency, vCL^2/K. However, other relevant dimensionless frequencies emerge for the two-step effect depending on the value of $\bar{G}$.

The phase angle results for $\bar{G}$ between 10 and 500, shown in Fig. 6(a), follow a general trend. For a range of dimensionless frequency values, the phase angle, at low values, is on the Fourier reference curve but smaller at larger values of frequency. When $\bar{G}$ is very large, the phase angle for the two-step model has nearly the same value as the Fourier conduction model and it is nearly independent of $\bar{C}$. As $\bar{G}$ decreases, the phase angle further departs from the expected Fourier phase angle and the dependence of the phase angle on $\bar{C}$ becomes detectable. Figure 6(b) shows the dimensionless amplitude at $x = L$ caused by the periodic surface heat flux. The amplitude is nearly the same as that for the Fourier conduction model and the logarithmic scale is for clarity of presentation. The results for $\bar{G}$ of about five or less are plotted in Figs 7(a–b). The phase angle, ϕ, in Fig. 7(a), shows a stronger dependence on $\bar{C}$ and the dimensionless temperature amplitude, Fig. 7(b), assumes higher values than those of the Fourier conduction model. Note that, in Fig. 7(a), the phase angle can be less for $\bar{G} = 5$ than for $\bar{G} = 1$. This behavior occurs when electrons transport a larger portion of energy across the layer in comparison to molecular communications due to the Fourier conduction. Indeed, a linear variation suggested modification of dimensionless frequency in Figs 6 and 7 when $\bar{G}$ is small.

An examination of equation (24) shows that, in

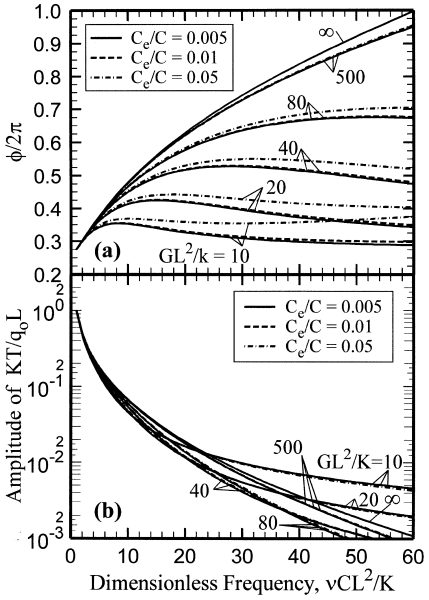

Fig. 6. The variation of (a) the phase angle, ϕ, and (b) the dimensionless amplitude with dimensionless frequency, vCL^2/K, for GL^2/K between 10 and 500 and $\bar{C}$ between 0.005 and 0.05.

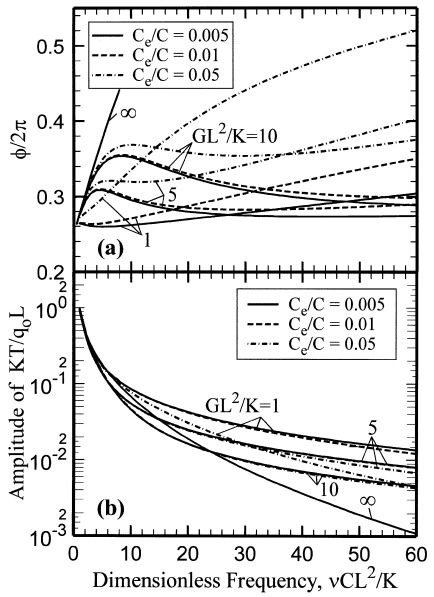

Fig. 7. The variation of (a) the phase angle, ϕ, and (b) the dimensionless amplitude with dimensionless frequency, $\nu CL^2/K$, for GL^2/K between one and ten and $\bar{C}$ between 0.005 and 0.05.

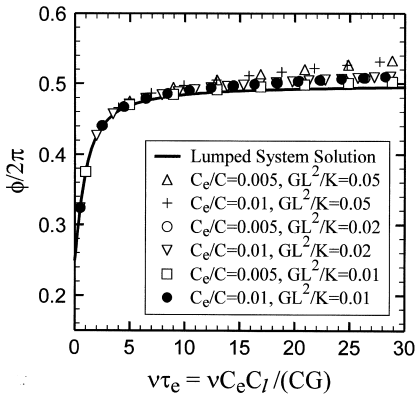

Fig. 8. The region of $GL^2/K < 0.05$ when the energy transport across a thin metal plate is by electrons.

addition to coordinates and time, the temperature and phase angle depend on $\bar{G}$, $\bar{C}$, and $\nu CL^2/K$. It is of practical interest to study the range of variables when the number of these parameters is reduced. As an example, when $\bar{G}$ is very small, Elsayed-Ali et al. [13] suggests setting $\nabla\cdot\mathbf{q} = 0$. After deleting $\nabla\cdot\mathbf{q}$ in equation (3a) and eliminating T_e using equation (2), the resulting differential equation has a form similar to equation (15), that is,

$$\frac{d^2 T_l}{d(t/\tau_e)^2} + \frac{dT_l}{d(t/\tau_e)} = \tau_e S/C \tag{25a}$$

whose solution is

$$T_l = \frac{\tau_t}{C}\left[\int_0^{t/\tau_t} S(\tau)\,d\tau - e^{-t/\tau_t}\int_0^{t/\tau_t} e^{\tau} S(\tau)\,d\tau\right] \tag{25b}$$

where the dummy variable of integration, τ, is dimensionless. When $S = q_0\sin(\nu t)$, the computation of the phase angle, using equation (25b), leads to $\sin(\phi) = (\nu\tau_e)/[1+(\nu\tau_e')^2]$ and $\cos(\phi) = -(\nu\tau_e)^2/[1+(\nu\tau_e)^2]$. The solid line in Fig. 8 shows the variation of the phase angle, $\phi = \tan^{-1}(-1/\nu\tau_e)$, as a function of $\nu\tau_e = \nu C_e C_l/(CG)$. The discrete data in the figure are computed using equation (24). For $\bar{G} = 0.05$, the deviations from the solid line, at $\nu\tau_e = 5$, is only 1.3%, whereas, for $\nu\tau_e = 5$ increases to 5.3%, and the error is much lower for smaller $\bar{G}$ values. This good agreement indicates that, for $\bar{G} < 0.05$, there are negligible thermal gradients in the lattice and the electron gas. In general, when $\nu\tau_e = 2\pi$ or less, the period is of the order of electron relaxation time and the solid line in Fig. 8 is a good approximation. This regime, where the thermal conduction is negligible, is analogous to a lumped system in Newtonian heating where t/τ_e is related to $\bar{G}\,Fo = (GL^2/K)(Kt/C_eL^2)$ that plays the role of Biot number $\times$ Fourier number. When $\bar{G} > 0.05$, Fig. 8, the deviation from the solid line increases; however, the results remain insensitive to $\bar{C}$. To demonstrate the contribution of $\bar{G}$, Fig. 9 is prepared by extracting $\bar{G}$ from the dimensionless frequency used in Fig. 8. Figure 9 shows that the phase angle, for values of $0.05 \leqslant \bar{G} \leqslant 5$, depends on $\nu C_e C_l L^2/(KC)$ and $\bar{G}$ but remains independent of $\bar{C}$ until $\bar{G} = 5$ and $\bar{C} = 0.05$. The phase angle response for this dimensionless frequency is further explored in ref. [14].

4. Conclusion and remarks

Thin films and short heat flux times offer special challenges for modeling thermal behavior. Below some maximum length and time interval, the Fourier heat conduction no longer serves as an accurate description of temperature and heat flow fields. It is remarkable that there is a unified solution for metallic, nonmetallic, and various other substances. This type of solution is mathematically simple to obtain because it uses Fourier conduction eigenfunctions and many of these eigenfunctions are available in the literature [15]. Except for the term in the curly brackets, equation (19a) or (19b) is the Green's function that is valid for homogeneous materials. The two cases studied show a difference in the nature of phase angles, the thermal wave model shows higher phase angles while the two-step model shows lower phase angles than the Fourier conduction model. A thermal wave may exist in dielectric material. However, in the case of the

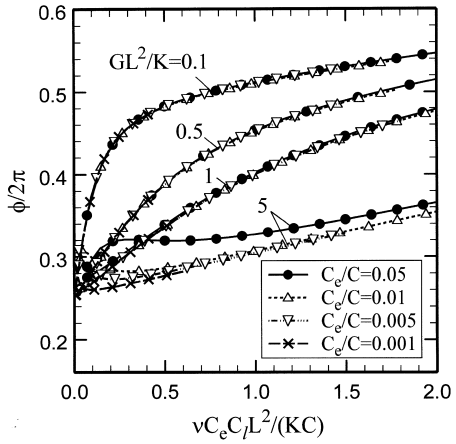

Fig. 9. The variation of the phase angle, ϕ, with dimensionless frequency, $vC_eC_lL^2/(KC)$, for GL^2/K between 0.1 and 5 and $\bar{C}$ between 0.001 and 0.05.

parabolic two-step model, since $C_l > C_e$ and $\tau_q \cong 0$, the argument of the hyperbolic sine in equation (24) is positive; hence, there is no thermal wave in a metallic film.

As discussed earlier, the phase delay in a dielectric material depends on vCL^2/K and Sp. When $Sp < 20$, there will be a detectable increase in phase shift due to the finite thermal wave speed and, when $Sp < 10$, this contribution is significantly larger. In principle, the phase angle can be detected in nonmetallic substances of small thickness with relatively small values $\sigma L/\alpha$.

The phase angle results of the numerical simulation, Figs 6–9, indicate the interesting mechanisms of heat conduction. For Fourier heat conduction, the lattice and electron temperature remain in local equilibrium. Fourier heat conduction would be expected as G (or $\bar{G}$) approaches infinity. For large values of $\bar{G}$, Fig. 6, the phase angle response is essentially Fourier and independent of $\bar{C}$ and $\bar{G}$. As $\bar{G}$ reduces to 10, the variable $\bar{G}$ begins to greatly influence the phase angle, however, the influence of $\bar{C}$ remains relatively small. The effect of $\bar{C}$ becomes significant, Fig. 7, when $\bar{G}$ approaches one and the effect of the Fourier conduction begins to diminish. For $\bar{G}$ below 0.05, Fig. 8, the contribution of the Fourier conduction diminishes and the phase angle depends on a single parameter. In this regime, the heat transfer can be considered wholly two-step with the transfer of energy being from electrons to lattice in the non-equilibrium state for all the frequencies investigated. Figure 9 describes a transition regime where the influence of the thermal conduction is small but graphically detectable.

The phase angles apparently have a minimum limit at 0.25, or a 90° phase difference for the two-step parabolic, Fourier, and thermal wave models. For the thermal wave model and Fourier model, this minimum is seen only at the lowest frequencies. The minimum phase angle is approached at higher frequencies for some combinations of $\bar{G}$ and $\bar{C}$ in the two-step model results.

Based on the results of numerical simulations, experimental determination of $\bar{G}$ and $\bar{C}$ could be accomplished using this model. Presently, single frequency modulation of laser irradiance is difficult to accomplish; the multiple frequency input is the most feasible. Metal films varying in thickness could be tested and the phase angles compared to results of the two-step model shown here. The multiple frequency input could be analyzed for phase information and compared with the phase information of the resulting temperature variation.

4.1. Wave phenomenon in the solution

Depending on the values of τ_q and τ_t, the temperature described by equation (18c) can exhibit wave behavior. For example, when $\tau_t = 0$ and $\tau_q > 0$, the arguments of hyperbolic sine and cosine can become imaginary indicating existence of a wave phenomenon; in contrast, there is no wave if $\tau_q = 0$ and $\tau_t > 0$. The existence of a wave phenomenon, $\beta_n^2 - \lambda_n^2 < 0$, leads to a condition

$$\left(\frac{\tau_q + \tau_e}{\tau_t}\right)(\gamma_n\tau_t) > \frac{1}{4}[1 + (\gamma_n\tau_t)]^2. \tag{26}$$

The right-hand-side and the left-hand-side of inequality (26) are plotted as a function of their common variable, $\gamma_n\tau_t$, in Fig. 10. The right-hand-side of inequality (26) describes a parabola shown in Fig. 10 while the left-hand-side represents a family of lines passing through the origin with a slope equal to $\mu = (\tau_q + \tau_e)/\tau_t$. A line through the origin with slope of 1 is tangent to the solid line in Fig. 10 indicating that there is no thermal wave when $\mu = (\tau_q + \tau_e)/\tau_t < 1$; e.g., for metals, $\mu \cong C_e/C \ll 1$. In contrast, for dielectric materials, $\tau_t \to 0$ and $\mu \to \infty$, and the inequality (26) leads to $\tau_q\gamma_n > 1/4$, a condition for occurrence of the thermal wave.

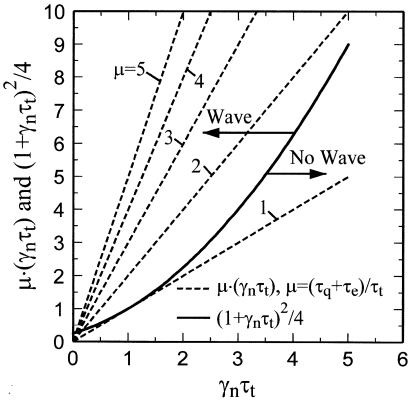

Fig. 10. Graphical representation of thermal wave condition in microscale heat conduction.

Acknowledgements

The work was supported by Texas ARP, Grant No. 003656–087, NSF, Grant No. CTS-9400647, and the University of Texas at Arlington.

Appendix

Examples 1 and 2 describe the behavior of dielectric materials and pure metals when there is a periodic heat input at one surface. The temperature solution of equation (18b), retaining τ_q, τ_t, and τ_e, and defining the parameters $a_m = \gamma_m - \beta_m$, $\gamma_m = (m\pi/L)^2 K/C$, and $\omega_m = (\beta_m^2 - \lambda_m^2)^{1/2}$ is

$$\frac{KT}{q_0 L} = \sum_{m=0}^{\infty} \frac{(2-\delta_{0m})\cos(m\pi x/L)}{\omega_n(\tau_e+\tau_q}$$

$$\times \{(\Lambda_1 + v\tau_q\Lambda_2)\exp[-a_m Kt/(CL^2)] + (\Gamma_{s1} + v\tau_q\Gamma_{s2})\sin(vt) + (\Gamma_{c1} + v\tau_q\Gamma_{c2})\cos(vt)\}/ [v^4 + (a_m^2 - \omega_m^2)^2 + 2v^2(a_m^2 + \omega_n^2)] \quad \text{(A1)}$$

where

$$\Lambda_1 = v[2a_m\omega_m\cosh(\omega_m t) + (v^2 + a_m^2 + \omega_m^2)\sinh(\omega_m t)] \quad \text{(A2)}$$

$$\Lambda_1 = [\omega_m(v^2 - a_m^2 + \omega_m^2)\cosh(\omega_m t) - (v^2 + a_m^2 - \omega_m^2)\sinh(\omega_m t)] \quad \text{(A3)}$$

$$\Gamma_{s1} = \Gamma_{c2} = -\omega_m(v^2 - a_m^2 + \omega_m^2) \quad \text{and} \quad \Gamma_{c1} = -\Gamma_{s2} = -2va_m\omega_m. \quad \text{(A4)}$$

The periodic terms in equation (A1) can be cast in the form $\sin(vt-\phi)$ where ϕ is the phase angle.

References

[1] C.L. Tien, J.H. Lienhardt, Statistical Thermodynamics, McGraw-Hill, New York, 1979.

[2] T.Q. Qui, C.L. Tien, Short-pulse laser heating on metals, International Journal of Heat and Mass Transfer 35 (1992) 719–726.

[3] T.Q. Qui, C.L. Tien, Heat transfer mechanisms during short-pulse laser heating on metals, ASME Journal of Heat Transfer 115 (1993) 835–841.

[4] Da Yu Tzou, The generalized lagging response in small-scale and high-rate heating, International Journal of Heat and Mass Transfer 38 (1995) 3231–3240.

[5] Kathy J. Hays-Stang, A. Haji-Sheikh, Phase delay using periodic heat flux in thin films, in: V. Prasad et al. (Eds.), ASTME STD-Vol. 323, ASME New York, 1996, pp. 111–119.

[6] C. Kittel, Introduction to Solid State Physics, 6th ed., John Wiley and Sons, New York, 1986, pp. 139–141.

[7] F.P. Incropera, D.P. DeWitt, Fundamentals of Heat and Mass Transfer, 3rd ed., John Wiley and Sons, New York, 1990.

[8] A. Haji-Sheikh, J.V. Beck, Green's function solution for thermal wave equation in finite bodies, International Journal of Heat and Mass Transfer 37 (1994) 2615–2626.

[9] M.N. Ozisik, D.Y. Tzou, On the wave theory in heat conduction, ASME Journal of Heat Transfer 116 (1994) 526–535.

[10] J.I. Frankel, B. Vick, M.N. Ozisik, Flux formulation of hyperbolic heat conduction, Journal of Applied Physics 58 (1985) 3340–3345.

[11] D.W. Tang, N.Araki, Non-Fourier heat conduction in a finite medium under periodic surface thermal disturbance, International Journal of Heat and Mass Transfer 39 (1996) 1585–1590.

[12] Kathy J. Hays-Stang, A. Haji-Sheikh, An analytical solution for heat transfer in thin films, in: S.T. Thynell, A.F. Emery (Eds.), ASMT HTD-Vol. 293, ASME, New York, 1994, pp. 1–7. 14.

[13] H.E. Elsayed-Ali, T.B. Norris, M.A. Pessot, G.A. Mourou, Time-resolved observation of electron–phonon relaxation in copper, Physical Review Letters 58 (1987) 1212–1215.

[14] Kathy J. Hays-Stang, A. Haji-Sheikh, Periodic heat flux temperature phase difference for thin metal films, in: Goodson et al. (eds.), ASME HTD-VOL. 354, ASME, New York, 1997, pp. 205–212.

[15] J.V. Beck, K.D. Cole, A. Haji-Sheikh, B. Litkouhi, Heat Conduction Using Green's Functions, Hemisphere Publishing Corp., Washington, DC, 1992.